BRNO UNIVERSITY OF TECHNOLOGY

VYSOKÉ UČENÍ TECHNICKÉ V BRNĚ

FACULTY OF MECHANICAL ENGINEERING

FAKULTA STROJNÍHO INŽENÝRSTVÍ

INSTITUTE OF PHYSICAL ENGINEERING

ÚSTAV FYZIKÁLNÍHO INŽENÝRSTVÍ

ULTRAFAST LASER-INDUCED CONTROL OF MAGNETIC MATERIALS

ULTRARYCHLÁ LASEREM INDUKOVANÁ KONTROLA MAGNETICKÝCH MATERIÁLŮ

BACHELOR'S THESIS

BAKALÁŘSKÁ PRÁCE

AUTHOR

AUTOR PRÁCE

Jakub Opršal

SUPERVISOR

VEDOUCÍ PRÁCE

M.Sc. Jon Ander Arregi Uribeetxebarria, Ph.D.

BRNO 2022

BRNO UNIVERSITY OF TECHNOLOGY
FACULTY OF MECHANICAL ENGINEERING

Assignment Bachelor's Thesis

Institut:	Institute of Physical Engineering
Student:	**Jakub Opršal**
Degree programm:	Physical Engineering and Nanotechnology
Branch:	no specialisation
Supervisor:	**M.Sc. Jon Ander Arregi Uribeetxebarria, Ph.D.**
Academic year:	2021/22

As provided for by the Act No. 111/98 Coll. on higher education institutions and the BUT Study and Examination Regulations, the director of the Institute hereby assigns the following topic of Bachelor's Thesis:

Ultrafast laser–induced control of magnetic materials

Brief Description:

There is currently significant interest in finding mechanisms for energy–efficient magnetization control at the nanoscale via magnetic fields, electrical and spin currents, or optical excitation. This bachelor thesis will investigate the utilization of ultrashort laser light pulses (~ 100 femtoseconds) to manipulate the magnetization state of magnetic thin films. Femtosecond light pulses can induce demagnetization, magnetization switching, or magnetic phase transitions in thin–film systems. Imaging magnetic domain configurations via magneto–optical microscopy before and after laser illumination will enable identifying the laser–induced processes for different light parameters (e.g., fluence or polarization).

Bachelor's Thesis goals:

1. Literature research of the state–of–the–art on the topic and related methodologies.
2. Optimizing and developing a laser setup for illumination of magnetic thin films under tunable light parameters (polarization, wavelength, energy per pulse).
3. Performing magneto–optical imaging of magnetic domain configurations in thin films before and after pulsed laser light illumination.

Recommended bibliography:

SOLDATOV, I. V., a SCHÄFER, R. Selective sensitivity in Kerr microscopy. Review of Scientific Instruments. 2017. 88, 073701. ISSN 1089-7623. Dostupné z: doi:10.1063/1.4991820

BEAUREPAIRE, E., MERLE, J.-C., DAUNOIS, A., a BIGOT, J.-Y. Ultrafast Spin Dynamics in Ferromagnetic Nickel. Physical Review Letters. 1996. 76, 4250. ISSN 1079-7114. Dostupné z: doi:10.1103/PhysRevLett.76.4250

MANGIN, S., et al. Engineered materials for all-optical helicity-dependent magnetic switching. Nature Materials. 2014, 13, 286. ISSN 1476-4660. Dostupné z: doi:10.1038/nmat3864

Deadline for submission Bachelor's Thesis is given by the Schedule of the Academic year 2021/22

In Brno,

L. S.

prof. RNDr. Tomáš Šikola, CSc. Director of the Institute	doc. Ing. Jaroslav Katolický, Ph.D. FME dean

Abstrakt
Magnetické materiály jsou ve velkém používány pro ukládání dat, která jsou zapisována ve formě bitů pomocí externího magnetického pole. Dlouho se věřilo, že doba potřebná pro změnu magnetizace je v řádu desítek až stovek pikosekund. Revoluční experiment v roce 1996 položil základ pro nový obor ultrarychlého ovládání magnetických materiálů, řádově zkracující čas potřebný pro změnu magnetizace. Mimo jiné ukázal, že magnetizace materiálu může být ovlivněna i světelnými pulzy. V této práci jsme replikovali fundamentální, laserem indukované experimenty ve ferromagnetických a ferrimagnetických materiálech. Postavili jsme optickou sestavu schopnou provádět tyto experimenty pro různé polarizace světla. Tato variabilita umožňuje rozlišit různé mechanismy a jevy, které se vyskytují při ultrarychlém ovládání magnetizace magnetických materiálů.

Summary
Magnetic materials are widely used for digital data storage. Data are written in form of bits using external magnetic field. It was long thought that magnetic materials could not be controlled faster than tens to hundreds of picoseconds. A breakthrough experiment in 1996 paved the way for a new field, showing that light can also controlled with femtosecond laser pulses and in the order of picoseconds. Here, we replicate fundamental laser-induced all-optical switching experiments in ferromagnetic and ferrimagnetic materials. Ultrafast laser setup was developed to perform such experiments with different light polarization. Thanks to this, we can distinguish different mechanism and different phenomena present for ultrafast control of magnetic materials.

Klíčová slova
Ultrarychlý magnetismus, přepínání magnetizace laserovými pulzy, femtosekundový pulzní laser, závislost na kruhové polarizaci, nezávislost na kruhové polarizaci, polarizace světla, magneto-optický Kerrův jev, magnetické multivrstvy

Keywords
Ultrafast magnetism, all-optical switching, femtosecond laser pulses, helicity-dependent, helicity-independent, light polarization, magneto-optical Kerr effect, magnetic multilayers

OPRŠAL, J. *Ultrarychlá laserem indukovaná kontrola magnetických materiálů.* Brno: Vysoké učení technické v Brně, Fakulta strojního inženýrství, 2022. 35 s. Vedoucí M.Sc. Jon Ander Arregi Uribeetxebarria, Ph.D.

I declare that I have written my bachelor's thesis on the theme of *Ultrafast laser-induced control of magnetic materials* independently, under the guidance of the supervisor, M.Sc. Jon Ander Arregi Uribeetxebarria, Ph.D. and using the sources quoted in the list of literature at the end of the thesis.

Jakub Opršal

I would like to thank my supervisor M.Sc. Jon Ander Arregi Uribeetxebarria, Ph.D. for his guidance and his never-ending patience. He helped me with every step of the way and always answering even the most stupid questions asked multiple times. My sincerest thanks goes to my colleague Alexander Velič for sample preparation. Without them I would be truly lost.

I would like to thank my classmates and friends. Without them I would not be able to come so far.

Huge thanks goes to my family for always supporting me and forcing me to finish.

I would also like to thank Ceitec nanomagnetism group, especially Ing. Vojtěch Uhlíř Ph.D.

Part of this work was carried out with the support of CEITEC Nano Research Infrastructure (ID LM2015041, MEYS CR, 2016–2019), CEITEC Brno University of Technology.

Jakub Opršal

Contents

Introduction **1**

1 Magnetism **5**
1.1 Magnetization . . . 5
1.2 Magnetic susceptibility and magnetic ordering . . . 5
1.2.1 Exchange interaction . . . 6
1.2.2 Magnetostatic energy . . . 8
1.2.3 Zeeman energy . . . 8
1.2.4 Magnetocrystalline and shape anisotropy . . . 8
1.3 Hysteresis . . . 10

2 Polarization optics and magneto-optics **11**
2.1 Electromagnetic wave propagation . . . 11
2.2 Polarization of light and Jones calculus . . . 12
2.2.1 Alternative coordinate system . . . 13
2.2.2 Polarization ellipse . . . 13
2.2.3 Jones matrices for optical elements . . . 14
2.3 Magneto optical Kerr effect . . . 14
2.3.1 Dielectric tensor . . . 15
2.3.2 Fresnel coefficients and reflection matrix . . . 15
2.3.3 Geometries of the Kerr effect . . . 16

3 Ultrafast laser setup **17**
3.1 Laser source . . . 17
3.2 Laser setup for polarization-dependent illumination experiments . . . 17

4 Magneto-optical characterization of Co/Pt and Co/Gd samples **21**
4.1 Sample overview . . . 21
4.2 Static characterization . . . 22

5 Laser-induced magnetization switching **27**
5.1 Helicity-dependent magnetization switching in Co/Pt . . . 27
5.2 Helicity-independent magnetization switching in Co/Gd . . . 28

Conclusion **31**

References **33**

List of abbreviations **35**

Introduction

Overview of ultrafast control of magnetic materials

The modern world relies heavily on computers. Thanks to this, we create huge amounts of data which need to be stored and manipulated. This puts emphasis on ways the data are stored. So far, we used magnetic materials controlled by magnetic field to write bits. Nowadays, the majority of digital information is stored in magnetic storage media, where the information writing is done using external magnetic fields. In 1996 a revolutional experiment was done by Beaurepaire and Bigot [1].

It was shown that when illuminating a thin film of ferromagnetic Ni using high-power femtosecond laser pulses it was possible to demagnetize the sample within the first 500 fs from the arrival of the pulse. The time-resolved evolution of magnetization was followed by measuring the magneto-optical Kerr effect of the Ni film in a pump-probe setting (see Figure below). This work showed for the first time that manipulation of magnetic materials in the timescale of one picosecond and below is possible, introducing the research field of ultrafast magnetism.

To understand the ultrafast demagnetization, a three-temperature model was introduced, consisting of three reservoirs: electrons, spins and lattice (phonons) [1]. The pulse initially excites the electrons by adding heat to the system, transferring a large amount of energy to the system and driving it into non-equilibrium state. It then dissipates into the system consisting of lattice and, and because the energy transfer rate between those reservoirs are not symmetric, it can be concluded that the spins react faster than lattice. The equilibrium is reached after several picoseconds [2].

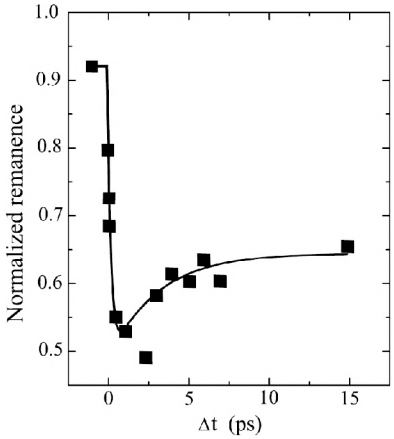

Discovery of the ultrafast demagnetization phenomenon in Figure. Graph shows remanent magnetization as a function of the delay of the probe. Taken from [1]

These studies were further expanded by Stanciu *et al.* [3] and an additional landmark discovery was made in 2007 - the ability to not only demagnetize a magnetic sample using light, but also to control its magnetization orientation. Light pulses of different polarization were used on a $Gd_{22}Fe_{74.6}Co_{3.4}$ alloy. It was shown that the light helicity has a different effect depending on the magnetization orientation. Experiments were done without the presence of external magnetic field, opening interesting route to magnetic-field free control of magnetization and subsequently writing information using light. Laser was

scanned across an area with different out-of-plane orientation of magnetization for linear, left circular and right circular polarization, depicted in figure below. For right-circular polarization, the illuminated samples region with M- (down) magnetization switches its direction while M+ (up) magnetized areas show no response, and vice versa for left circular polarization. This phenomenon was name as all-optical helicity dependent switching (HD-AOS) of magnetization. Linearly polarized pulses cause the area to demagnetize, causing formation of oppositely oriented domains with both up and down orientation.

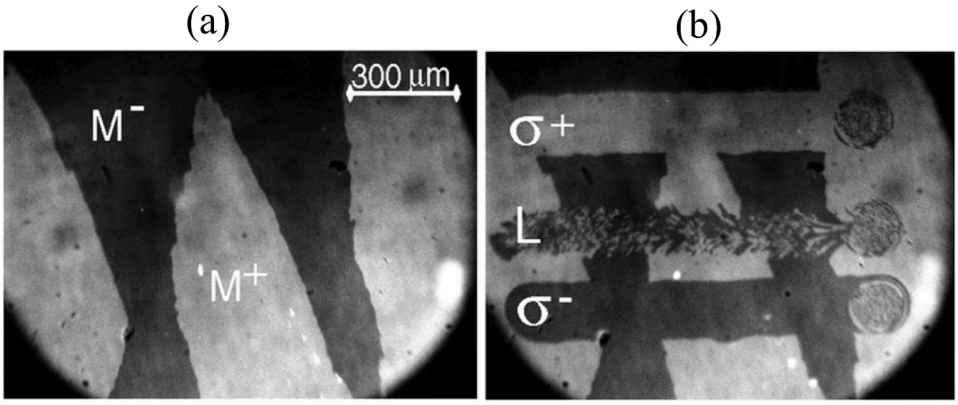

Pioneering experiment showing all-optical helicity dependent switching on GdFeCo alloy. Taken from [3]

Follow up study performed by Radu *et al.* [4] obtained further details of underlying physical phenomena in AOS. For alloy films with the same elements but slightly different composition $Gd_{25}Fe_{65.6}Co_{9.4}$ they found that magnetization switch is possible using only linearly polarized light, indicating all-optical helicity independent switching (HI-AOS). It is yet to be fully understood the true nature of HI-AOS but it was thought that the phenomena is exclusively occurring in ferrimagnets.

GdFeCo s experience ferrimagnetic ordering, with two sublattices of Gd and FeCo. Magnetizations of those sublattices are antiparallel and when the system is illuminated with ultrafast laser pulses, demagnetization occurrs at different rates in each sublattice (Gd moments demagnetize slower than FeCo [4]). Subsequently, this is causing the magnetization to switch [5]. Lalieu *et al* [6] continued in the study of ferrimagnets with the study of Co/Gd bilayers. They perform experiments showing single pulse is capable of HI-AOS as they shone a laser at the same spot and change the number of pulses, showing that an odd number of pulses causes the magnetization to switch while an even number has left the spot in the initial configuration. The effect was observed independently of the initial magnetization of the sample. This process is usually

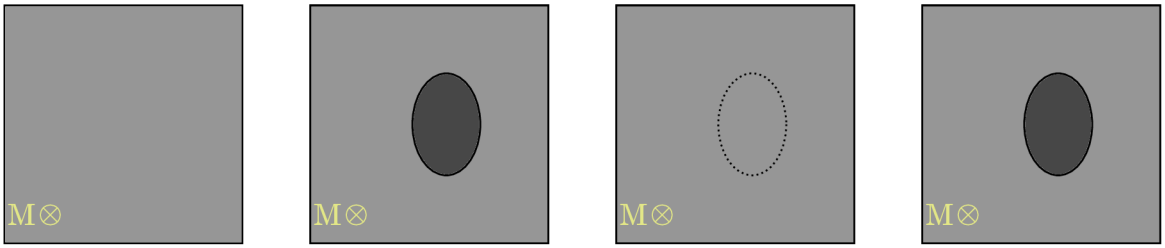

Schematic of single-pulse experiment using linearly polarized light pulses which shows helicity-independent all-optical switching on ferrimagnetic materials. Showing that an number of pulses switches the magnetization back to its original state.

On top of that, they measured minimal fluence (energy per area) needed for the magnetization switch, further expanding the idea that the process is, among other things, thermally driven.

Among others, Lambert *et al* [7] studied HD-AOS for ferromagnetic Co/Pt multilayers. It was also shown that linearly polarized light can demagnetize the sample, creating random domains.

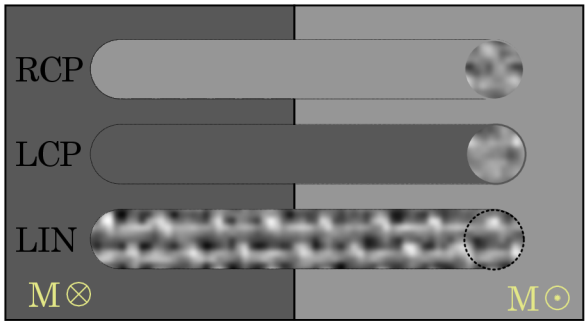

Schematics of all-optical helicity-dependent switching for ferromagnets. Sample is scanned three times with different polarization. It shows that magnetization switches based on the helicity of used light. Linearly polarized light demagnetizes the area by creating domains pointing both up and down. Circle on the right of each denotes a place where the laser was stationary for a longer period of time, causing the area to demagnetize due to increase in temperature.

This prompted two different approaches to all-optical switching (AOS) with ferrimagnets and ferromagnets and it was shown that AOS does not depend on the type of magnetic ordering [5]. Other types of structures have been studied, however, such as rare earth-transitional metal alloys [8] and multilayers [9].

Thesis overview

In this thesis, we focus on basic magnetism and describe different types of magnetic ordering in chapter 1. With this we characterize the samples in chapter 4. Further, we examine polarization optics in chapter 2 to be subsequently used in the laser setup development as described in 3. Finally, we preform for laser induced control of magnetic materials and observe different process, both thermal and non-thermal, causing the magnetization to switch 5

1. Magnetism

Firstly, we will discuss elementary magnetic quantities such as magnetization and susceptibility to help us define basic magnetic properties and differentiate between certain types of magnetic ordering. Next, we will focus on magnetic energies and interactions, allowing us to understand even wider range of different magnetic properties.

1.1. Magnetization

After applying external magnetic field $\mathbf{H}$ (commonly known as auxiliary field), the response of a material is described by magnetic induction (magnetic field) $\mathbf{B}$. For each material the relationship between $\mathbf{B}$ and $\mathbf{H}$ is unique and intrinsic property. In some, we observe that $\mathbf{B}$ is linear function of $\mathbf{H}$ (also in free space). However, in more general case we can link these vectors by equation

$$\mathbf{B} = \mu_0(\mathbf{H} + \mathbf{M}), \tag{1.1}$$

where μ_0 is the permeability of free space and $\mathbf{M}$ is the magnetization of a material, defined as total magnetic dipole moment $\mathbf{m}$ per unit volume

$$\mathbf{M} = \frac{\sum \mathbf{m}}{V}. \tag{1.2}$$

Magnetization is by definition property of material depending on the structure, more specifically on ions, atoms, and molecules from which the material consists, but also on the interaction between them [10].

1.2. Magnetic susceptibility and magnetic ordering

For further study of magnetic materials, it will be beneficial to introduce another quantity with which we can describe some magnetic properties, especially when external field is applied. Apart from magnetization mentioned earlier, susceptibility is introducing the relationship between $\mathbf{H}$ and $\mathbf{M}$

$$\chi = \frac{\mathbf{M}}{\mathbf{H}}. \tag{1.3}$$

Susceptibility can tell us how responsive material is to an applied field. Armed with this knowledge we can introduce other types of magnetic ordering in materials: diamagnetic, paramagnetic, and antiferromagnetic [10].

Diamagnetic materials

Diamagnetism is the response of some material to external field. It can be understood using the analogy of an atom with an orbiting electron. Among other forces acting on the electron, the one arising from Faraday effect is the most important. When field is applied, an induction current is generated. Lenz's law states that the nature of the induced current is in the opposite direction. The magnetic moment generated by this current is pointing

in the opposite direction of the applied field. Hence increasing the energy of the system and causing the material to be pushed out of the magnetic field.

Paramagnetic materials

Unlike the diamagnetic materials, paramagnets consist of atoms with nonzero angular momentum. Their microscopic magnetic moment is non-zero, however, moments are oriented randomly, therefore the net magnetization is zero. After applying external magnetic field, moments start to align with it. After we remove the external field, the magnetization drops to zero again. For some paramagnets, the susceptibility is inversely proportional to temperature [10].

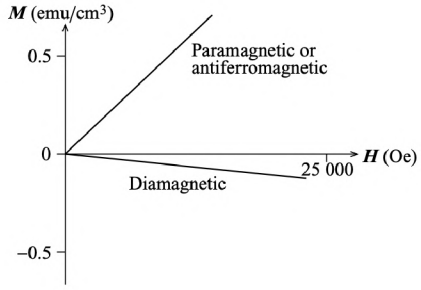

Figure 1.1: Graph showing different dependence of **M** on **H** for diamagnets, paramagnets and antiferromagnets. Adopted from [10]

1.2.1. Exchange interaction

As stated above, the interactions between between atoms play a significant role in magnetization of medium. That is again linked to auxiliary field and as a consequence creates an effective field $\mathbf{H}^{\mathrm{i}}$. This was first described by Weiss when he introduced the so called molecular field $\mathbf{H}_{\mathrm{w}}$, linearly proportional to magnetization

$$\mathbf{H}_{\mathrm{w}} = \gamma \mathbf{M}. \tag{1.4}$$

γ is the mollecular field constant. Therefore the total field acting on medium is given as

$$\mathbf{H}^{\mathrm{i}} = \mathbf{H}_{\mathrm{ext}} + \mathbf{H}_{\mathrm{w}}. \tag{1.5}$$

The nature of said field can be traced to exchange interaction which combines Coulomb repulsion and Pauli principle. With this in mind, if we consider electron as a primary source of magnetic moment, we know no two electrons can be in a same state, thus their spin must differ. In this configuration, the electrons have antiparallel spins. For parallel orientation of spins the electrons must occupy different states. This tells us that electrons with parallel spins can be found on different orbits, therefore the Coulomb interaction will be smaller while for antiparallel arrangements of spins their wavefunctions will overlap, making the Coulomb repulsion more prominent.

States represented by different quantum numbers corresponds to different energies, from this we can conclude that there must be an energy difference depending which we can expressed as

$$\varepsilon = -2\frac{\mathcal{J}}{\hbar^2}\,\mathbf{s}_1 \cdot \mathbf{s}_2. \tag{1.6}$$

This would be true for a single H_2 molecule, however for many electron spins constrained to lattice Heisenberg generalized formula for energy (hamiltonian) as

$$\mathbf{E}_{ex} = -\sum_{ij} \mathcal{J}_{ij}\,\mathbf{S}_i \cdot \mathbf{S}_j. \tag{1.7}$$

$\mathbf{S}_i$ and $\mathbf{S}_j$ represent dimensionless spin operators and $\mathcal{J}_{ij}$ is the exchange integral. If $\mathcal{J}_{ij} < 0$ then the interaction is ferromagnetic, trying to align spins parallel and if $\mathcal{J}_{ij} > 0$ the interaction is antiferromagnetic with spins aligned antiparallel with respect to one. These crucial phenomenas we shall discuss next.

Ferromagnets

As mentioned above, ferromagnetic materials, thanks to exchange energy, tend to orient neighbouring magnetic moments parallel to each other. This means that even when no external field is applied they exhibit magnetic properties. Their typical reaction to external field is well described by a hysteresis loop. Thanks to their nature, a specific temperature exists, called Curie temperature T_C. When heated above this temperature, material looses its magnetic properties as the vibrations caused by thermal energy are so strong that order is disturbed.

Antiferromagnets

In antiferromagnetic materials neighbouring atoms have spins pointing antiparallel to each other. Thanks to this behaviour, their magnetization in zero field is also zero. Essentialy, the crystal is split into two sublattices, each with its own direction for magnetization. Applied field causes the moments to orient in the direction of field, similar to paramagnets. Above certain temperature T_N (Néel temperature) the thermal energy is greater than exchange and spins start to have random orientation and material undergoes a phase transtition from antiferromangetic state to paramagnetic state [11].

Ferrimagnets

Ferrimagnets in a sense combine properties of ferromagnets and antiferromagnets. Firstly, they tend to have their magnetic moments aligned antiparallel due to exchange energy. They are also comprised of two sublattices, but each sublattice has a different magnetization, resulting in net magnetization of a material. Ferrimagnets also have a characteristic temperature T_M Compensation temperature. As the magnetization of these two sublattices depend differently on temperature, there is one point, before reaching Curie temperature, where both magnetizations are the same in magnitude but pointing opposite of each other, resulting in zero magnetization of a material. Apart from alloys, ferrimagnetic-like structure can be also observed in multilayer structure such as Co/Gd. The thin layer of Co with magnetic moment induces magnetization in the neighbouring layers of otherwise paramagnetic Gd, thus coupling the atoms into an antiferromagnetic state [6].

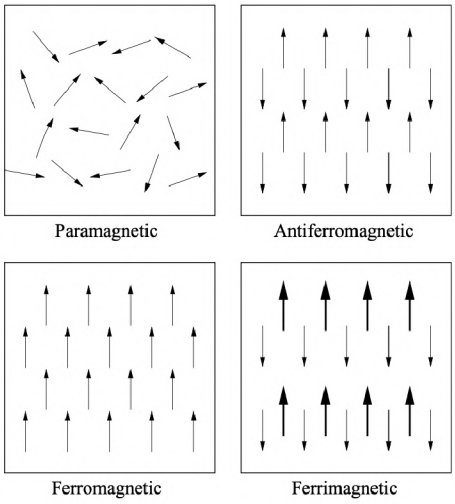

Figure 1.2: Overview of different magnetic ordering. Taken from [10]

1.2.2. Magnetostatic energy

Origins of magnetostatic energy comes from a simple dipole–dipole interaction. This interaction can be viewed as an interaction between moment $\mathbf{m}_i$ in a field $\mathbf{B}_j$ created by $\mathbf{m}_j$. Then the magnetostatic energy is given as

$$E_m = -\frac{1}{2}\sum_{\substack{i,j \\ i\neq j}} \mathbf{m}_i \cdot \mathbf{B}_j. \tag{1.8}$$

For a continuous medium the equation can be rewritten as

$$E_m = -\frac{1}{2}\int_V \mu_0 \mathbf{M} \cdot \mathbf{H}_d \, dV, \tag{1.9}$$

where $\mathbf{H}_d$ is the field created in the sample and we integrate over the sample [11].

1.2.3. Zeeman energy

Force exerted by magnetic field on a current is always perpendicular to its motion ($\mathbf{v}\times\mathbf{B}$), therefore we cannot associate any potential energy with such force. Instead, we only study work done by magnetic field on temporary electric field created by dipole.
Firstly, let us consider magnetic dipole $\mathbf{m}$ in an external field $\mathbf{B}$. Torque on such dipole exerted by the field is $\mathbf{M} = \mathbf{m}\times\mathbf{B}$. Incremental change in energy is given as $\mathrm{d}E = \mathbf{M}\mathrm{d}\theta'$. Then the energy depending on angle between the vectors [11] is

$$E_z = -\mu_0 \int_V \mathbf{M} \cdot \mathbf{H}_{ext} \, dV. \tag{1.10}$$

1.2.4. Magnetocrystalline and shape anisotropy

When talking about ferromagnets, we must mention anisotropy, as the effect of magnetic properties being dependent on the direction in which the magnetization is oriented (easy

axis). Without this property, there would not be any ferromagnets to speak of. In crystal structures, there are multiple axes along which the magnetization can be oriented. Generally following one of the directions in crystal structure given by material and lattice [12]. We can associate anisotropy energy with a material's tendency to have its magnetization pointing in an easy axis as

$$E_a = \int_V K_1 \sin^2 \theta \, dV. \tag{1.11}$$

θ is the angle between anisotropy axis and $\mathbf{M}$ and K_1 is a constant taking into account shape and temperature and in units $\mathrm{J\,m^{-3}}$ [11]. For the study of thin films, it is necessary to take into account the structure of used samples. Apart from the magneto-crystalline anisotropy for bulk material, the effect of interface or surface starts to affect the thin sample's dipole orientation. If the surface anisotropy is strong enough, it can change the direction of the easy axis. Direction of dipoles can be then switched from the direction given by the lattice to be perpendicular to the surface of a thin film. We can define effective anisotropy K_{eff} which combines the anisotropy of bulk material as well as the surface anisotropy [13]

$$K_{eff} = K_V + \frac{2K_S}{t}, \tag{1.12}$$

where t is the thickness of thin film. Alternative form of this equation displays linear dependency of effective anisotropy on film thickness

$$K_{eff} \cdot t = K_V t + 2K_S. \tag{1.13}$$

When plotted, it shows the existence of a thickness for which the moments change their orientation from perpendicular to the surface to parallel to the surface.

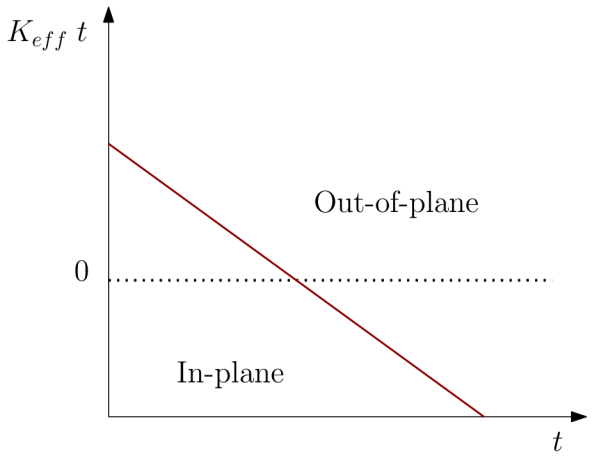

Figure 1.3: Schematics of anisotropy per area on thickness of film. Intersection between line and zero denotes a point where the prefferential axis changes from in-plane to out-of-plane.

1.3. Hysteresis

Hysteresis is a phenomenon closely tied with ferromagnets and their property of having magnetization even when no external field is applied. However, when field is applied, we can observe a nonlinear reaction of **M** to **H** until the so-called saturation M_s is reached, meaning that spontaneous magnetization can no longer increase and all moments are aligned in the direction of the field. Coercive field H_c corresponds to field needed to reverse the effect of **H** and to make the magnetization zero. Remanence M_r is the magnetization still present after applied field is zero.

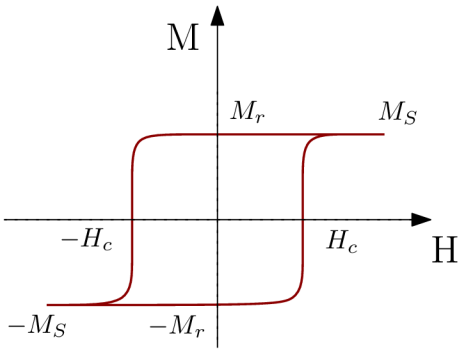

Figure 1.4: Hysteresis curve typical for ferromagnets and ferrimagnets. Specific points along hysteresis are marked: saturation magnetizatiom M_S, coercive field H_c and remanent magnetization M_r

2. Polarization optics and magneto-optics

Here we study how light propagates in free space and how it interacts with media. We discuss polarization optics and Jones calculus. Magneto-optical effects are introduced for basic understanding of Kerr microscopy and later used for characterization of samples and visualization of experiments.

2.1. Electromagnetic wave propagation

For optics in general, but especially for wave optics, Maxwell's equations are the fundamental relation connecting fields and charges

$$\nabla \cdot \mathbf{D} = \rho \tag{2.1a}$$
$$\nabla \cdot \mathbf{B} = 0 \tag{2.1b}$$
$$\nabla \times \mathbf{E} = -\frac{\partial \mathbf{B}}{\partial t} \tag{2.1c}$$
$$\nabla \times \mathbf{H} = \mathbf{j} + \frac{\partial \mathbf{D}}{\partial t}. \tag{2.1d}$$

This is the most general form of Maxwell's equations, for optics we consider free space, meaning no free charge ($\rho = 0$) and no current density ($\mathbf{j} = 0$). For cases where this condition cannot be applied, we need a way to describe the relationship between the aforementioned fields. We can use this set of equations [14]

$$\mathbf{D} = \varepsilon_0 \boldsymbol{\varepsilon} \mathbf{E} = \varepsilon \mathbf{E} + \mathbf{P} \tag{2.2a}$$
$$\mathbf{B} = \mu_0 \boldsymbol{\mu} \mathbf{H} = \mu_0 (\mathbf{H} + \mathbf{M}). \tag{2.2b}$$

where $\boldsymbol{\mu}$ is permeability tensor and $\boldsymbol{\varepsilon}$ is dielectric (permitivity) tensor, which we will discuss more in Section 2.3. Both are second rank tensors. As mentioned, for electromagnetism in free space we omit any media dependence and set $\boldsymbol{\mu} = \boldsymbol{\varepsilon} = \hat{1}$. With this in mind, and with free space in consideration, we can take the curl of equation 2.1c and time derivative of 2.1d, when we combine them we get

$$-\nabla \times \nabla \times \mathbf{E} = \mu_0 \varepsilon_0 \frac{\partial^2 \mathbf{E}}{\partial t^2}, \tag{2.3}$$

therefore eliminating $\mathbf{H}$ and with mathematical identity $\nabla \times \nabla \times \mathbf{A} = \nabla(\nabla \cdot \mathbf{A}) - \Delta \mathbf{A}$ [15] (keeping in mind 2.1a) we have the wave equation of light for $\mathbf{E}$

$$\Delta \mathbf{E} = \mu_0 \varepsilon_0 \frac{\partial^2 \mathbf{E}}{\partial t^2}. \tag{2.4}$$

An analogous approach could be taken to eliminate $\mathbf{E}$ and obtain a wave equation for $\mathbf{H}$. In both cases $\frac{1}{\sqrt{\mu_0 \varepsilon_0}}$ denotes the speed of light in vacuum. For most materials we can consider $\boldsymbol{\mu} = 1$ for visible and near-infrared light because such light corresponds to a

frequency of hundreds of THz, meaning the oscillations are so fast the spins cannot react. Therefore the material's response is guided by $\boldsymbol{\varepsilon}$ alone.
One of the functions satisfying 2.4 is that of a plane wave, in complex notation proportional to $\exp[i(\mathbf{k}\cdot\mathbf{r}-\omega t)]$. Where $\mathbf{k}$ is wave vector defining direction of propagation of wave and ω is the frequency. If we use this expression again in Maxwell's equations, we find that $\mathbf{E}$ is always perpendicular to $\mathbf{k}$ and $\mathbf{H}$ [15]. This is crucial for next section in which we will introduce a formalism based on this result.

2.2. Polarization of light and Jones calculus

Polarization describes the behavior of $\mathbf{E}$ when light is propagating through free space or non-absorptive media. In principle, we could use also $\mathbf{H}$ as these two are linked. We can express polarization as a 2D vector. Assuming the light travels along the z axis it can be represented by a superposition of two waves one oscillating along x axis and the other along y axis, using matrix representation [15], this can be written as

$$\mathbf{E} = \begin{pmatrix}\mathbf{E}_x\\ \mathbf{E}_y\end{pmatrix} = \begin{pmatrix}E_{0x}e^{i\phi_1}\\ E_{0y}e^{i\phi_2}\end{pmatrix}. \tag{2.5}$$

This notation is called Jones vector. Another useful way of describing light is normalized Jones vector which is obtained from original by dividing it by $\sqrt{|E_{0x}|^2+|E_{0x}|^2}$ and factoring out common factors [14].
Depending on the amplitudes of said waves and their phase shift, there are several states how the resulting wave can be polarized. Firstly, unpolarized light, for which the electric field changes randomly. Next, we will describe states with unique relations of phase and amplitude.

Linear polarization

For $|E_{0x}|, |E_{0y}| \in \mathbb{R}$ and phase difference $\phi = \phi_1 - \phi_2 = 0, \pi$ the light is linearly polarized. Jones vector corresponding to linear polarization $\begin{pmatrix}E_{0x}\\ E_{0y}\end{pmatrix}$ and E is oscillating along a line rotated by an arbitrary angle ψ with respect to x axis.

Circular polarization

If condition $|E_{0x}| = |E_{0y}| \in \mathbb{C}$ is satisfied and phase difference is $\phi = \phi_1 - \phi_2 = \pm\frac{\pi}{2}$ the light is circularly polarized. When viewed against the direction of propagation we can described two orientations: left-circularly polarized (LCP) and right-circularly polarized (RCP). First corresponds to electric field rotating counterclockwise and phase difference $\phi = -\frac{\pi}{2}$, second to clockwise rotation and phase difference $\phi = \frac{\pi}{2}$. In Jones notation it is given as

$$\begin{pmatrix}E_0e^{i\phi_1}\\ E_0e^{i(\phi_1\pm\frac{\pi}{2})}\end{pmatrix} = E_0e^{i\phi_1}\begin{pmatrix}1\\ \pm i\end{pmatrix}. \tag{2.6}$$

Elliptic polarization

If amplitudes are complex and different in magnitude, the resulting polarization is elliptical. This state of polarization is the most general one apart from unpolarized light. The other mentioned above are just special cases of elliptical polarization. Linear for real amplitudes, circular for complex amplitudes equal in magnitude.

2.2.1. Alternative coordinate system

In some cases, it can be beneficial to describe polarized light, not in the standard coordinate system but rather use one which is more dependent on how the light propagates. Incident and reflected light create a plane perpendicular to some surface from which it is reflected, called the plane of incidence. Then light with polarization perpendicular to plane of incidence is said to be *s-polarized* from German "senkrecht" and light with polarization parallel to the plane of incidence is *p-polarized*, from German "parallel".

2.2.2. Polarization ellipse

To visualise the state of final polarization we can use ellipse, characterized by two angles: ψ determining the rotation of major axis, and χ determining the ellipticity (ration of minor to major axis). Using this tool we can quite easily understand different types of polarization mention above.

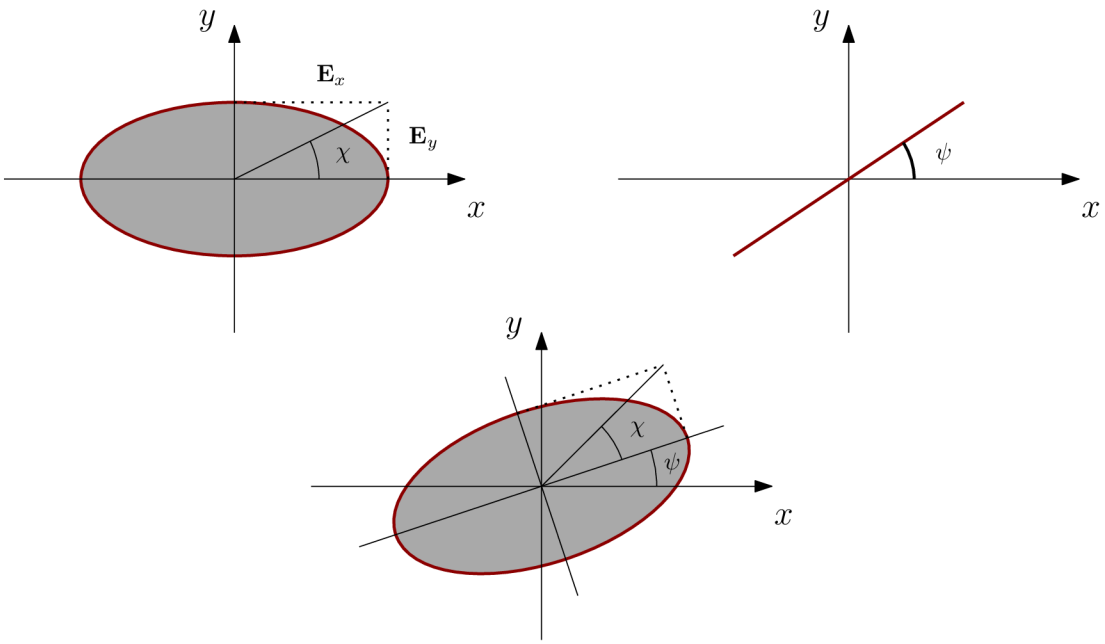

Figure 2.1: Top-left figure: definition of ellipticity χ. Top-right: definition of azimuth angle ψ for linear polarization. Bottom: visualisation of polarization of light using polarization ellipse. χ is the ellipticity, ψ is the azimuth angle and also the angle of rotation of major axis.

2.2.3. Jones matrices for optical elements

The main advantage of using Jones notation is in simulating how the light will behave when passed through a series of optical elements, each described by its own matrix. The final state of polarization of light is then given by multiplying the initial state represented by Jones vector by Jones matrices of corresponding elements

$$\mathbf{E}_f = \hat{\mathbf{J}}_3 \cdot \hat{\mathbf{J}}_2 \cdot \hat{\mathbf{J}}_1 \cdot \mathbf{E}_i. \tag{2.7}$$

This would represent a situation in which light passed through three elements in order: J_1, J_2, J_3. Absolutely essential element is linear polarizer described by Jones matrix [14]

$$\begin{pmatrix} \cos^2\theta & \cos\theta\sin\theta \\ \cos\theta\sin\theta & \sin^2\theta \end{pmatrix},$$

where θ is angle of rotation of polarizer with respect to x axis. The main use for a linear polarizer is selecting which polarization passes as only light oscillating in plane parallel to transmission axis of polarizer will be transmitted. For example system consisting of a single linear polarizer with fast axis parallel with y axis $\left(\begin{smallmatrix} 0 & 0 \\ 0 & 1 \end{smallmatrix}\right)$ will block incident light polarized along x axis $\left(\begin{smallmatrix} 1 \\ 0 \end{smallmatrix}\right)$.

Another wildly used elements may be phase retarders, specifically half-wave plate ($\lambda/2$) and quarter-wave plate ($\lambda/4$), each introducing phase shift of $\pi/2$ and $\pi/4$ respectively. Jones matrix for $\lambda/2$ is

$$e^{-\frac{i\pi}{2}} \begin{pmatrix} \cos^2\theta - \sin^2\theta & 2\cos\theta\sin\theta \\ 2\cos\theta\sin\theta & \sin^2\theta - \cos^2\theta \end{pmatrix}.$$

For $\lambda/4$ the expression reads [14]

$$e^{-\frac{i\pi}{4}} \begin{pmatrix} \cos^2\theta + i\sin^2\theta & \cos\theta\sin\theta - i\cos\theta\sin\theta \\ \cos\theta\sin\theta - i\cos\theta\sin\theta & \sin^2\theta + i\cos^2\theta \end{pmatrix}.$$

2.3. Magneto optical Kerr effect

During the years people have developed various ways to study magnetic properties of materials. For our purposes, the most important role play magneto optical effects, pioneered by Michael Faraday. He discovered that when linearly polarized light is passing through a glass media, which is placed into a magnetic field, the plane of polarization is rotated by some small angle, this is now called Faraday effect. However, for study magnetic properties of metals, there is another, more useful phenomena, analogous to Faraday effect, called Kerr effect. The main difference is that in Kerr effect we are interested in light reflected from a surface. This allows for a whole new field of microscopy where with just an optical microscope we are able to observe magnetic properties. The nature of both Kerr and Faraday effects arise from dielectric tensor being a linear function of magnetization of media. There also have been discovered effects depending on mangetization with its square such as Voigt effect [16].

2.3.1. Dielectric tensor

As we have discussed in section 2.1, Maxwell's equations describe fundamental behaviour both of magnetic and electric fields and charges. Unlike in optics, we now need to take into account free charges and current densities because we are interested in the materials response to field. This would be described by equation 2.2a. Here $\boldsymbol{\varepsilon}$ is now tensor of rank two not equal to identity matrix, instead, it can be broken down into separate components, each with unique dependence on magnetization [17]:

$$\hat{\boldsymbol{\varepsilon}} = \begin{pmatrix} \varepsilon_0 & 0 & 0 \\ 0 & \varepsilon_0 & 0 \\ 0 & 0 & \varepsilon_0 \end{pmatrix} + \begin{pmatrix} 0 & -iQm_3 & iQm_2 \\ -iQm_3 & 0 & iQm_1 \\ -iQm_2 & -iQm_1 & 0 \end{pmatrix}, \tag{2.8}$$

where the first component can be seen as the typical dielectric function, its only non-zero components are equal to the mentioned dielectric function and it is not dependent on magnetization in any way. Second component is linearly dependent on $\mathbf{m}$ and is the part that produces the rotation. Q is the Voigt constant and it describes the material strength of magneto-optical effects.
Wave equation, derived from 2.1, leads to two different solutions for n depending on helicity of propagation of waves [17]

$$n_{\pm} = \sqrt{\varepsilon_0}(1 \pm Q/2), \tag{2.9}$$

Where plus and minus subscript represents left or right circularly polarized light respectively. Important note here is that linearly polarized light can be also viewed as a superposition of two circularly polarized waves, one right and one left [14]. Armed with this knowledge, the basic idea behind Kerr effect can explained. Incident linearly polarized light is reflected but because it is comprised of RCP and LCP, which each experienece different n, the symmetry is broken and a phase shift is introduced between these two components, changing the light polarization from linear to elliptical.

2.3.2. Fresnel coefficients and reflection matrix

When the Maxwell's equations are solved with $\boldsymbol{\varepsilon}$ from equation 2.8 we get the following Fresnel coefficients [17]

$$r_{\mathrm{pp}} = \frac{n_0 \cos\vartheta_1 - n_1 \cos\vartheta_0}{n_1 \cos\vartheta_0 + n_0 \cos\vartheta_1} - \frac{\mathrm{i}2n_0 n_1 \cos\vartheta_0 \sin\vartheta_1 m_{\mathrm{x}} Q}{\left(n_1 \cos\vartheta_0 + n_0 \cos\vartheta_1\right)^2}, \tag{2.10a}$$

$$r_{\mathrm{sp}} = \frac{\mathrm{i}n_0 n_1 \cos\vartheta_0 \left(m_{\mathrm{z}} \cos\vartheta_1 + m_{\mathrm{y}} \sin\vartheta_1\right) Q}{\left(n_1 \cos\vartheta_0 + n_0 \cos\vartheta_1\right)\left(n_0 \cos\vartheta_0 + n_1 \cos\vartheta_1\right)\cos\vartheta_1}, \tag{2.10b}$$

$$r_{\mathrm{ss}} = \frac{n_0 \cos\vartheta_0 - n_1 \cos\vartheta_1}{n_0 \cos\vartheta_0 + n_1 \cos\vartheta_1}, \tag{2.10c}$$

$$r_{\mathrm{ps}} = -\frac{\mathrm{i}n_0 n_1 \cos\vartheta_0 \left(m_{\mathrm{z}} \cos\vartheta_1 - m_{\mathrm{y}} \sin\vartheta_1\right) Q}{\left(n_1 \cos\vartheta_0 + n_0 \cos\vartheta_1\right)\left(n_0 \cos\vartheta_0 + n_1 \cos\vartheta_1\right)\cos\vartheta_1}. \tag{2.10d}$$

n_1 and n_0 are the index of refraction for magnetic and nonmagnetic medium, respectively. In our case we set $n_0 = 1$ as we consider light propagating in air. ϑ_0 is the angle of incidence, ϑ_1 is the angle of refraction given by Snell's law and m_i are components

of magnetization. Using equations above we can write magneto-optical Fresnel reflection matrix that can tell us how the light will be polarized after reflected from a material, depending on angle of incidence

$$\hat{\mathbf{R}} = \begin{pmatrix} r_{ss} & r_{sp} \\ r_{ps} & r_{pp} \end{pmatrix}. \tag{2.11}$$

2.3.3. Geometries of the Kerr effect

Incident light together with light reflected from the sample define plane of incidence. With respect to magnetization orientation we can distinguish three configurations of Kerr effect: polar, with magnetization out-of-plane, longitudinal, with magnetization parallel with plane of incidence and transverse with magnetization perpendicular to the plane of incidence [18].

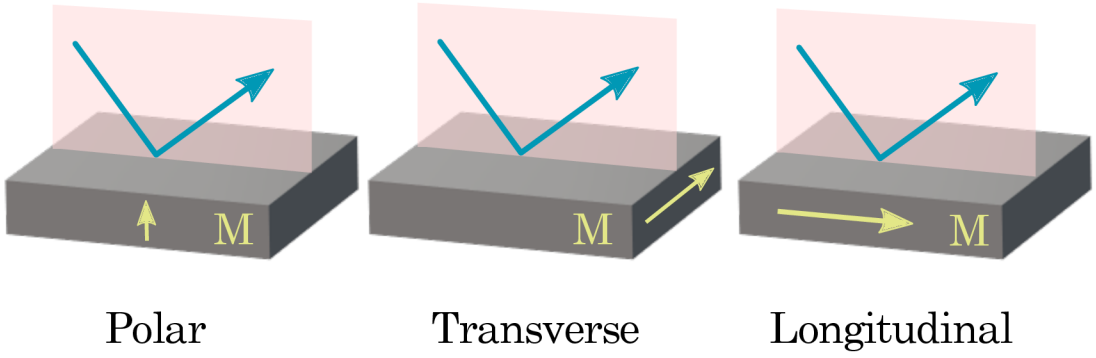

Figure 2.2: Different orientations possible for MOKE with respect to plane of incidence, defined by incoming and reflected light.

3. Ultrafast laser setup

In this chapter we will discuss femtosecond-laser-based optical setup employed for ultrafast control of magnetization, including its characteristics such as power, polarization, optical elements used and fluence.

3.1. Laser source

To obtain the pulses needed, we use a multiple components, starting with seed laser Monaco 1035-40-40 from Coherent, Inc. as a high-power pulse laser with pulse width $t_w < 350\,\text{fs}$. This fiber laser provides pulses of wavelength $\lambda = 1035\,\text{nm}$ and can provide power of 40 W at 1 MHz repetition rate which is adjustable between 10 kHz and 1 MHz [19].

Optical parametric amplifier Opera-F by Coherent, Inc., provides a range of wavelengths $650\,\text{nm} - 920\,\text{nm}$. Using nonlinear crystals to generate light of different frequencies and after an adjustable stage to generate the light of desired wavelength [20]. A pulse condenser located at the exit of Opera-F compresses the temporal width of the pulses provided by seed laser to $t_w \sim 40\,\text{fs} - 60\,\text{fs}$ depending on the wavelength.

For our experiments, we use a light output of 805 nm wavelength from the Opera-F. Pulse width was measured to be $\sim 40\,\text{fs}$. For our conditions we had 25 mW for 20 kHz repetition rate, giving us equivalent of 1.25 µJ per pulse. For scheme of the setup, the laser means sequence of just mentioned components, with fixed output parameters, which will for measurements remain constant.

3.2. Laser setup for polarization-dependent illumination experiments

Optical elements used for experimental setup for polarization-dependent laser experiments were deliberately chosen to accommodate the fact that we use pulse laser which introduces new challenges such as group delay dispersion. In general this means using thinner components compared to ones suitable for continuous laser. We used mirrors made by EKSMA Optics made for range of $760\,\text{nm} - 840\,\text{nm}$ before the second harmonic generation crystal (SHG), while after frequency doubling we employed optics suited to the $380\,\text{nm} - 420\,\text{nm}$ wavelength range. Firstly, the beam is split into two using beamsplitter (BS), for our experiments however, we only need the reflected part. SHG generates pulses of half the wavelength but reduces the power significantly, the upper limit of this process is 50 %. For focusing of the collimated beam we use plano-convex lenses with focal length 150 mm and after generation of 400 nm we again use a plano-convex lens with the same focal length to make the beam collimated again. Harmonic beamsplitter is then used to separate the two different wavelengths and light with 800 nm is reflected and then directed towards a beam trap. Transmitted light is then passed through a polarizer (P) and a quarter-wave plate (R), both mounted to rotating stands and the angle of quarter-wave plate can be precisely controlled with computer with Thorlabs' motorized rotational mount K10CR1/M

to switch between linear and RCP and LCP.

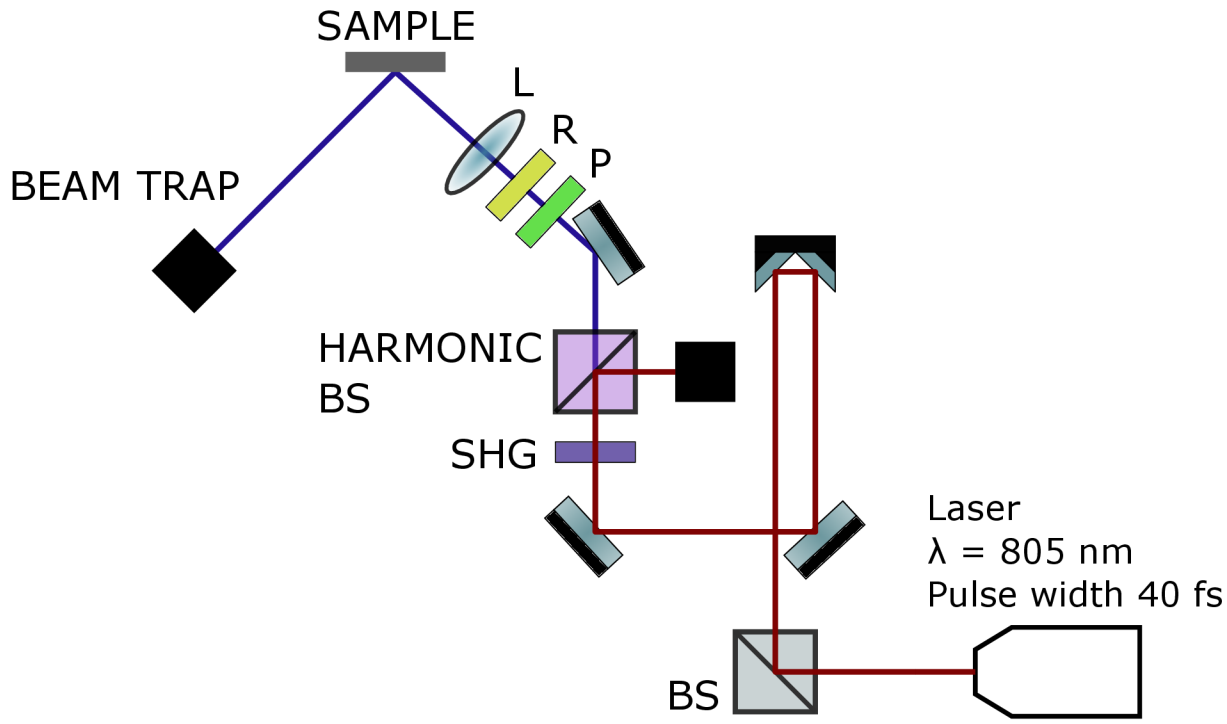

Figure 3.1: Experimental setup: infrared pulse laser, beamsplitter (BS), second-harmonic generation crystal used for generation of light with half the wavelength, harmonic beamsplitter used to separate the wavelengths, discarding the 805 nm, polarizer (P), quarter-wave plate (R) and a focusing lens (L).

We measured polarization just before the polarizer to be linear and rotated as seen in visualisation from polarimeter. Using this we can verify the ellipticity.

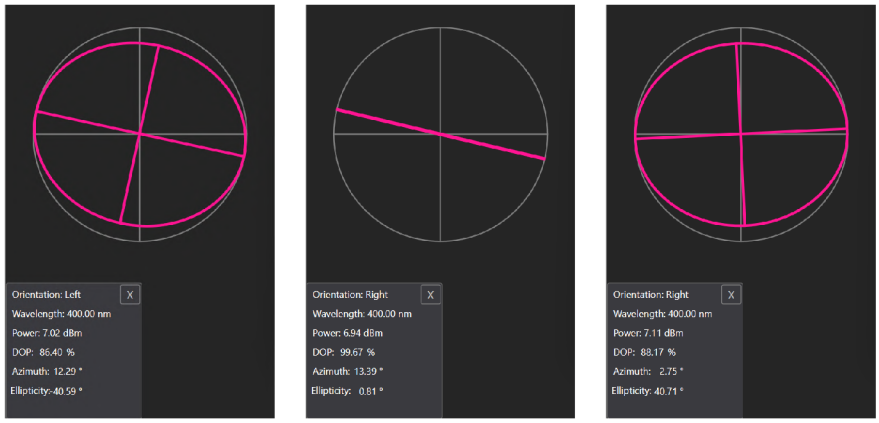

(a) (b) (c)

Figure 3.2: Measurements obtained from a Thorlabs' PAX1000 polarimeter for left circular, linear and right circular polarization.

The ideal ellipticity of circularly polarized state is $\chi = 45°$. In reality we measured $\chi = 40.59°$ for LCP and $\chi = 40.71°$ for RCP. In the case of linear polarization we would expect the ellipticity to be zero but the measurement showed $\chi = 0.81°$

Sample is mounted onto a stage with three motorized axes of motion allowing us to move it freely along x,y and z axes. In addition, a goniometer mounted to the stage, gives us the ability to make small angular adjustments, especially when directing the reflected pulses into a beam trap.

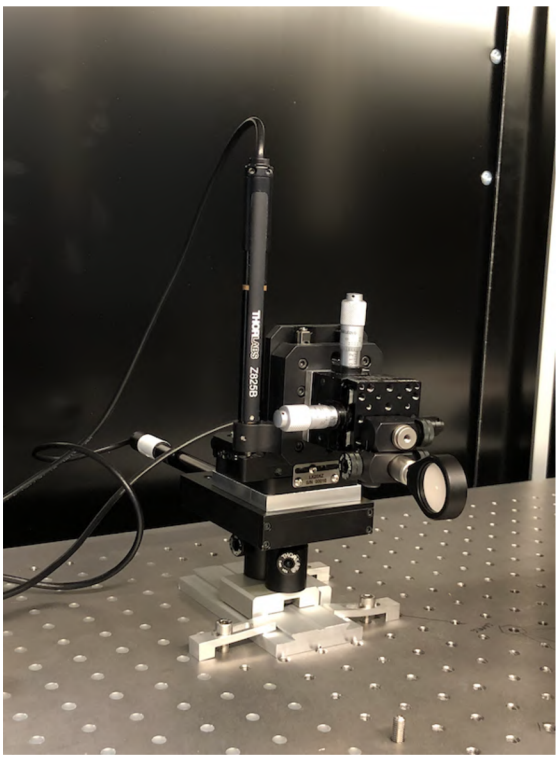

Figure 3.3: Motorized sample stage holder with mounted goniometer used for experiments.

Second-harmonic generation crystal

Crystals used for generation of second-harmonic utilizes nonlinear effects present in some materials such as BaB_2O_4. For weak electric fields or isotropic media the material's response $\mathbf{P}$ is a series of $\mathbf{E}$ [14]

For weak electric field, assuming a linear relationship between the electric polarization vector $\mathbf{E}$ and the electric vector $\mathbf{E}$ (linear medium approximation) is generally sufficient. However, for strong enough electric fields (such as in the case of a material interacting with a high-power ultrashort laser pulse), we write $\mathbf{P}$ as a sum of higher order contribution of $\mathbf{E}$ [14], with

$$\mathbf{P} = \varepsilon_0(\chi\mathbf{E} + \chi^{(2)}\mathbf{E}^2 + \chi^{(3)}\mathbf{E}^3 + ...), \tag{3.1}$$

where χ and χ^2 are the linear and quadratic susceptibility tensors. For strong enough electric fields, however, caused generally by a laser pulse, higher terms of $\mathbf{E}$ start to play more significant role. Assuming the field can be described as $\mathbf{E}_0 e^{-i\omega t}$ then the second term is producing higher harmonics, in this case with double the frequency but lower intensity. With this we are able to generate light with half the wavelength incident on SHG but with significantly reduced power.

4. Magneto-optical characterization of Co/Pt and Co/Gd samples

In this chapter we will discuss our samples of Co/Pt and Co/Gd and using MOKE microscopy study their properties, such as domain sizes and response to magnetic field for narrow part of the sample with respect to sample thickness and number of repetitions. These measurements were done to verify a well-defined perpendicular magnetic anisotropy (PMA) and a nearly-square hysteresis loop. Both are essential for later experiments done using ultrafast illumination. Samples used for experiments described in this thesis were fabricated by Alexander Velič and Jon Ander Arregi. All thicknesses mentioned in this chapter are in nanometers unless stated otherwise.

4.1. Sample overview

Ferromagnetic Co/Pt multilayers

Samples were prepared by magnetron sputtering and grown on a Si substrate with a thin Pt buffer layer: Si/SiO_x/Pt(3)/Co(t_{Co})/Pt(3)/Pt(2). We split different samples according to their Co thickness t_{Co} and number of repetitions N of [Co(t_{Co})/Pt(3)]$_N$.

Table 4.1: Summary of all used Co/Pt samples.

	Thickness of Co	
Repetitions	0.4	0.6
1x	[Co(0.4)/Pt(0.7)]	[Co(0.6)/Pt(0.7)]
3x	[Pt(0.4)/Pt(0.7)]$_3$	[Pt(0.6)/Pt(0.7)]$_3$
8x	[Pt(0.4)/Pt(0.7)]$_8$	

Ferrimagnetic Co/Gd bilayers

Similar to previous section, we have Co/Gd bilayer samples that were grown using magnetron sputtering in a way: substrate Si/SiO_x/Pt(4)/Co(t_{Co})/Gd(3)/Pt(2), we have two different thicknesses of Co 1.4 and 1.2 and the last layer of Pt protects the sample (so-called capping). The same structure and thicknesses were used by [6].

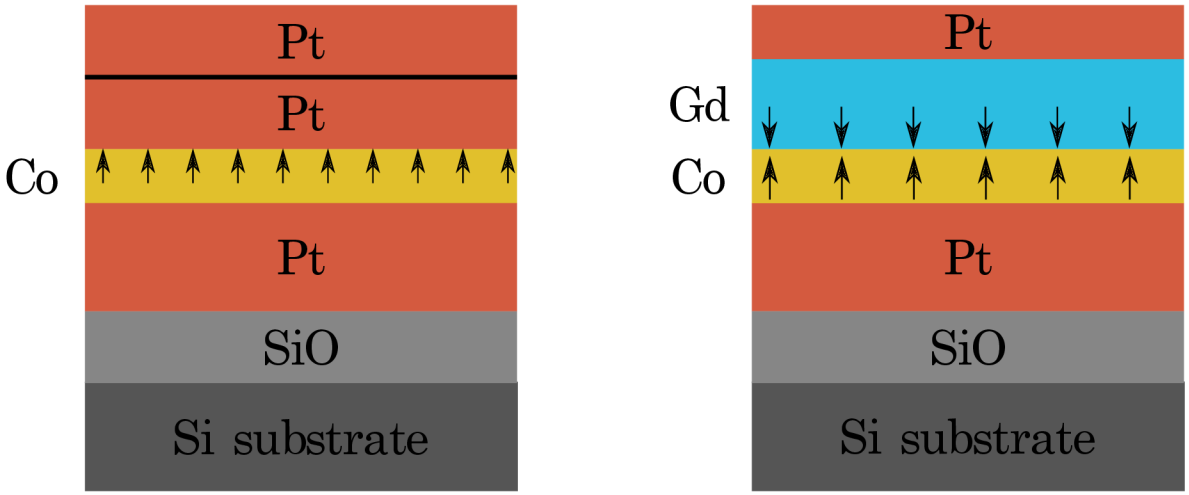

(a) (b)

Figure 4.1: Structure of the multilayer samples utilized in the experiments of this thesis. To grow Co/Pt with different repetition, we repeat the Co/Pt bilayer and always capped the sample with additional 2 nm of Pt. Capping provides protection from oxidation, similarly to Co/Gd. Arrows represent magnetic moments.

4.2. Static characterization

Our MOKE microscope has been implemented with a magnet so we can link state of the sample to the applied external field and thus acquire a hysteresis loop from a small region, given by the field of view of used objective. Furthermore, we can study the formation of magnetic domains and their propagation. Both Co/Pt and Co/Gd should have their magnetization out of plane due to PMA, hence the measurements using polar MOKE. In order to enhance the contrast, the shown images are obtained with respect to a subtracted reference state, usually defined in magnetic saturation. This allows enhancing the contrast produced by magneto-optical effects upon reorientation of magnetization and nucleation of magnetic domains. Every set of pictures shown corresponds to a hysteresis, denoting what field was applied.

Co/Pt

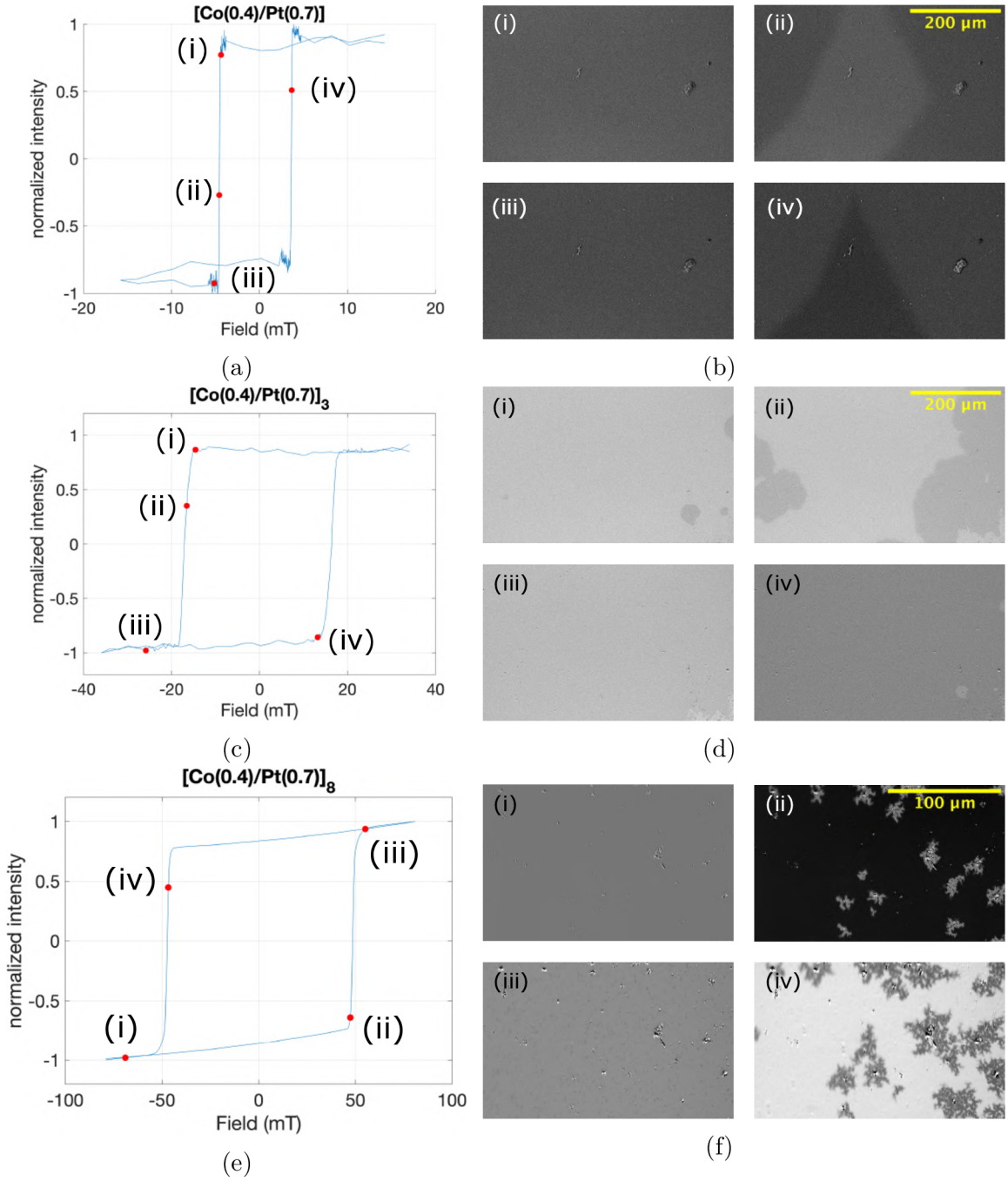

Figure 4.2: (a), (c), (e) Measurements of hysteresis from Kerr microscope for repetition $N = 1, 3$ and 8 with $t_{\mathrm{Co}} = 0.4\,\mathrm{nm}$. (b), (d), (f) visualization of domain formation for different repetitions in different fields. Each picture (i)-(iv) corresponds to a point denoted on hysteresis.

From the hysteresis measured for Co/Pt, there is clear dependence of field needed to fully magnetized sample to its cobalt thickness (in our case the repetition of Co/Pt bilayers). Increasing of Co thickness causes the domains' size decreasing [21]. The process of domain formation is driven by combination of energies: magnetostatic, which is dependent on the

volume and anisotropy, taking into account the surface effect as well as the interaction on interface. At one point, the energy needed to stay in fully saturated state is greater than that of a state broken into domains [22]. For repetition three times and more we can clearly observe formation of domains as they start to propagate from a point on a sample (nucleation point), a defect present on its surface.

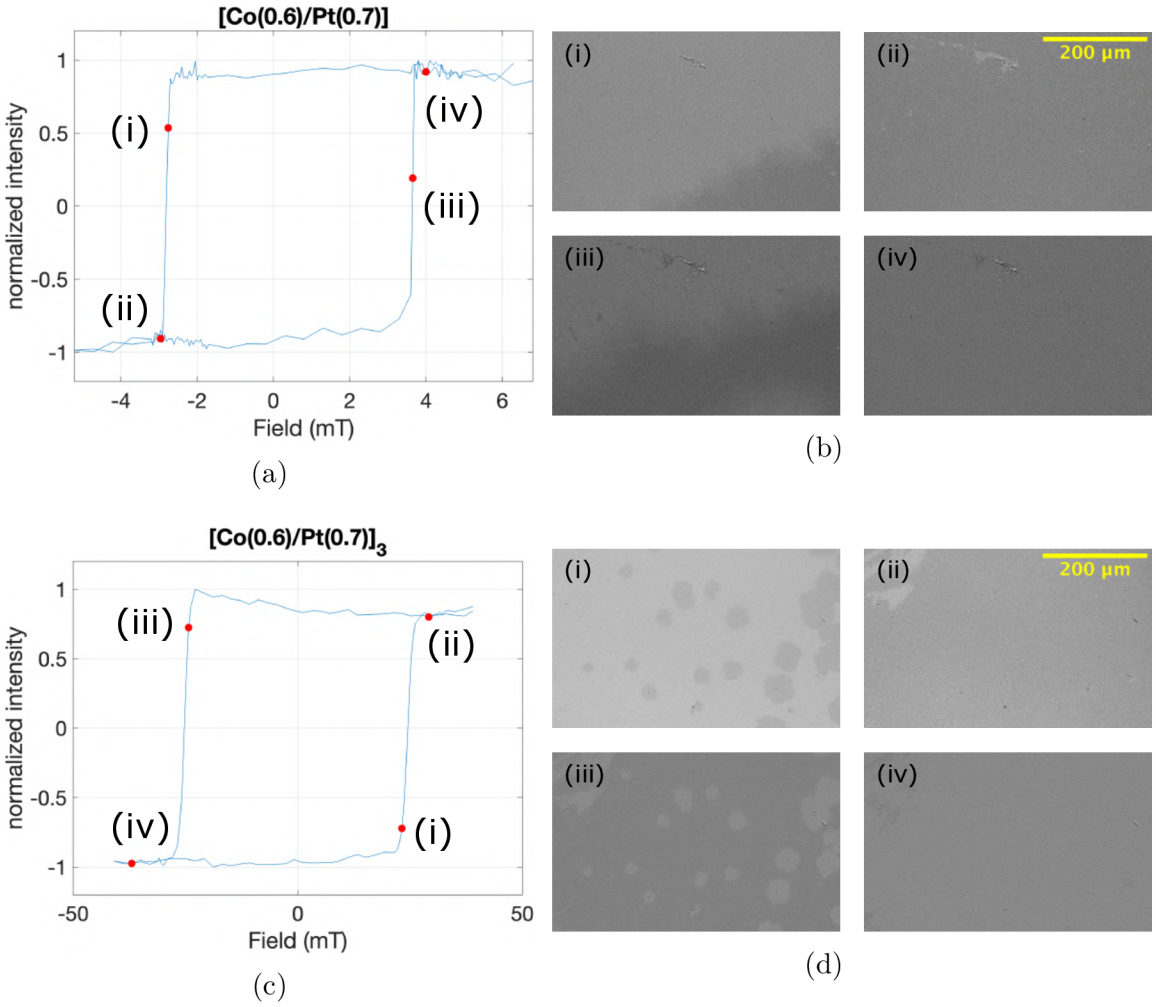

Figure 4.3: (a),(b) hysteresis obtained from Kerr microscope for for different repetition rates of Co/Pt multilayer, $t_{Co} = 0.6\,\text{nm}$. (b),(d) pictures of domain formation related to a magnetic field applied denoted on a hysteresis curve (i)-(iv).

Co/Gd

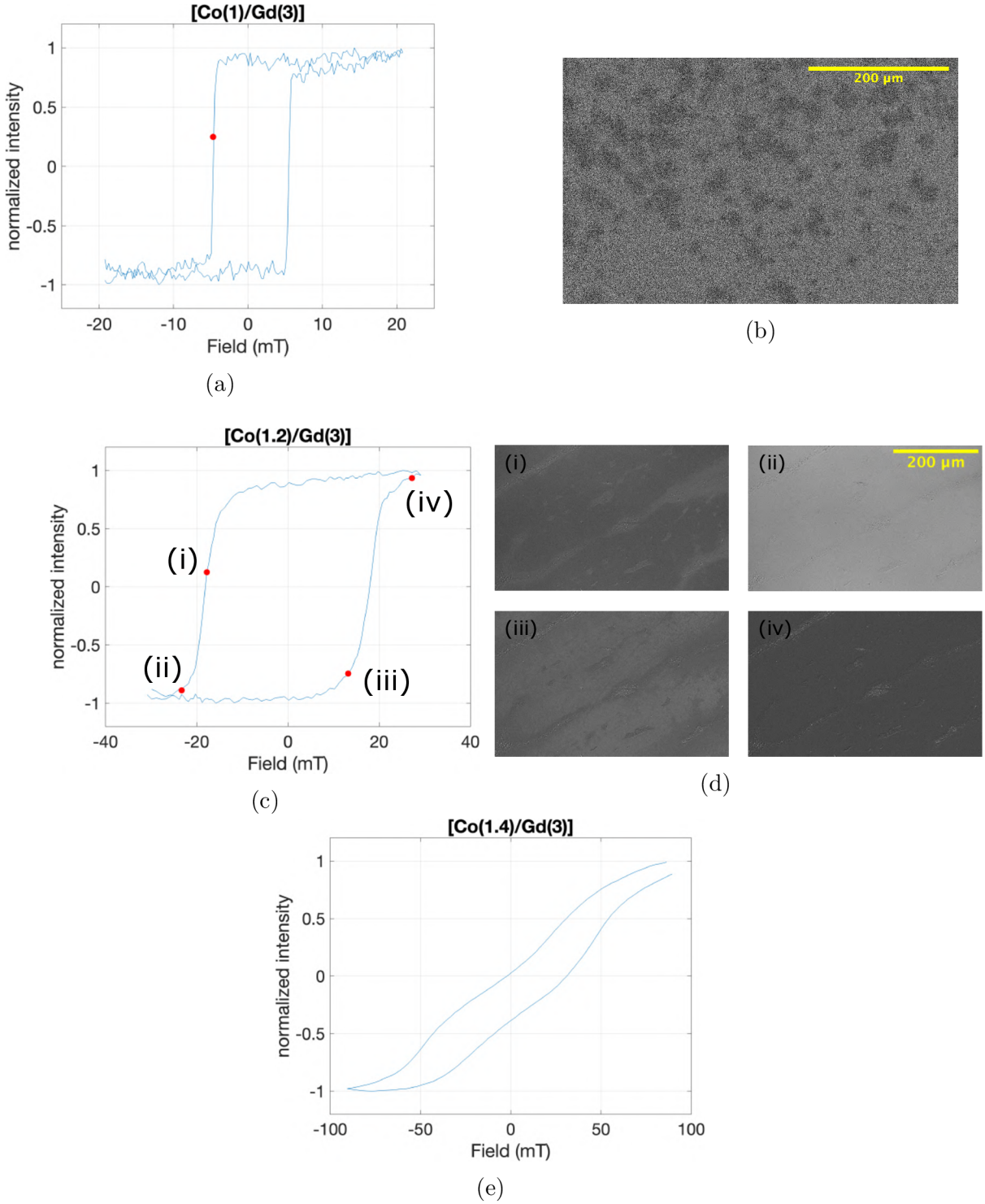

Figure 4.4: Measurement of hysteresis for Co/Gd multilayers with varying t_{Co} = 1, 1.2 and 1.4 nm. (a) only $t_{Co} = 1$ nm of all thicknesses showed square hysteresis, indicating strong perpendicular magnetic anisotropy and out-of-plane magnetization. With increasing t_{Co} magnetization had also in-plane component. (c) for $t_{Co} = 1.2$ nm small domains appeared but the hysteresis is affected by defects present on the surface and possibly by t_{Co} (i)-(iv). Pictures relate the domain formation for different fields applied. (e) we were not able to see any domains forming for $t_{Co} = 1.4$ nm.

Similar to Co/Pt, Co/Gd multilayers should experience perpendicular magnetic anisotropy causing out of plane magnetization, therefore we again measured polar MOKE. Notable is especially the result obtained for $t_{\mathrm{Co}} = 1.4\,\mathrm{nm}$, where the hysteresis does not follow the square profile expected from a sample with PMA. Even for $t_{\mathrm{Co}} = 1.2\,\mathrm{nm}$ the hysteresis is not square due to defects present on a sample surface as seen in figure 4.4d, where the defects require additional field, compared to the rest of the sample, to be applied for them to switch. This also corresponds to observations that for $t_{\mathrm{Co}} > 1\,\mathrm{nm}$, the PMA is not strong enough and the sample breaks into oppositely magnetized domains at zero applied, hence making them non-ideal samples for the laser-induced AOS experiments (because they do not retain magnetization at zero field) [9].

5. Laser-induced magnetization switching

Here we discuss measurements done using laser setup described in Chapter 3 for ultrafast control of magnetic multilayers, mainly the effects of different polarization of used pulses.

5.1. Helicity-dependent magnetization switching in Co/Pt

Co/Pt multilayers as shown in [7], up to certain power and number of repetition, experience HD-AOS. We were able to replicate this result on [Co(0.4)/Pt(0.7)]x3 multilayer. The sample was magnetized at 40 mT using the out-of-plane manget in the Kerr microscope setup. Laser was then swiped across two times, once with RCP, once with LCP. Repetition rate of laser was 20 kHz and power measured in the focal plane of focusing lens 3.75 mW giving us an energy of of 188 nJ per pulse. The laser sweeping speed was se to 0.5 mm s^{-1}. Sample is rotated 10° on vertical axis to prevent light coming back into the setup, however this means when scanning the whole sample is not in focal plane of focusing lens, causing a slight position dependent variation of the spot size (which it was estimated to be 60 µm-70 µm). For visualizing the result, MOKE microscope was used once again. When inspecting, only changes corresponding to the sweep line for RCP light are visible throughout the whole sample, indicating helicity-dependent switching. Upon closer inspection it is also visible that within the area illuminated, there are still small domains present, corresponding to the initial magnetization orientation, demonstrating that not all of the area switched magnetization. Applying field of 17 mT erases any changes made by the laser illumination and returns the sample to its original state, where we no longer see any contrast change.

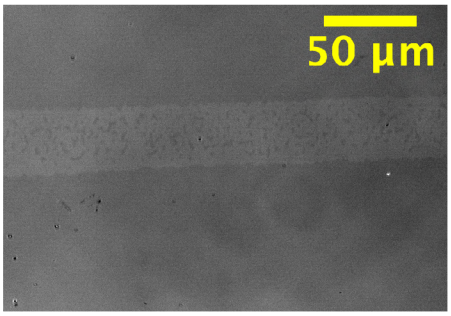

(a)

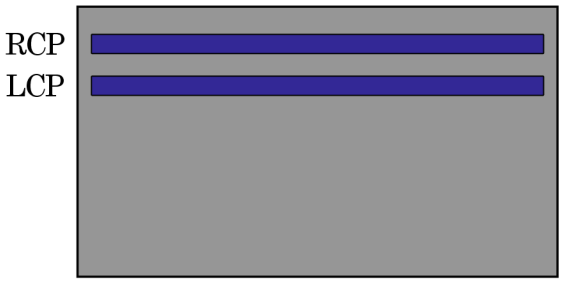

(b)

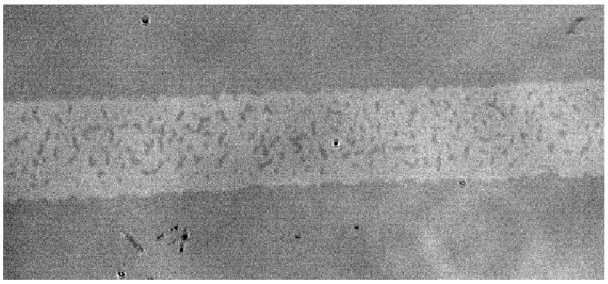

(c)

Figure 5.1: Laser scanned across a $[Co(0.4)/Pt(0.7)]_3$ sample with left- and right-circularly polarized (LCP and RCP) light. Magnetization switch is visible only for RCP light. Energy per pulse 188 nJ. (c) section of picture (a) with enhanced contrast. Distinguished domains visible within the area illuminated by laser.

5.2. Helicity-independent magnetization switching in Co/Gd

Similar experiment was done on Co/Gd multilayer with $t_{Co} = 1\,\text{nm}$. Sample was fully magnetized to 100 mT, speed of stage set to $0.1\,\text{mm}\,\text{s}^{-1}$ and stage was rotated 10° around vertical axis. Power was lowered to 1.2 mW using 20 kHz repetition rate, giving us 60 nJ per pulse. Given the ferrimagnetic-like structure of Co/Gd, the process for all-optical switching is different and helicty-independent as shown in [6]. This time, the sample was illuminated three times with LCP, RCP and linear polarization. The magnetization switch is visible in all three cases, however, the fraction of the switched area across the laser-illuminated area is different. This effect is described by magnetic circular dichroism, causing different absorption of light of LCP and RCP. It is clearly visible that for LCP used in Figure 5.2a, the portion of illuminated area switched is the lowest of the three polarizations, indicating lowest absorption of all. Linear light, as a superposition of both left and right circularly polarized light, has higher absorption and therefore larger area switched. Lastly, RCP absorbs the most, hence the portion of area switched is the largest. Pictures were again obtained in a Kerr microscope and for better visibility background was taken in an area where the laser was shone, then the sample was moved slightly to an area unaffected by the laser in order to enhance the contrast induced by the Kerr effect.

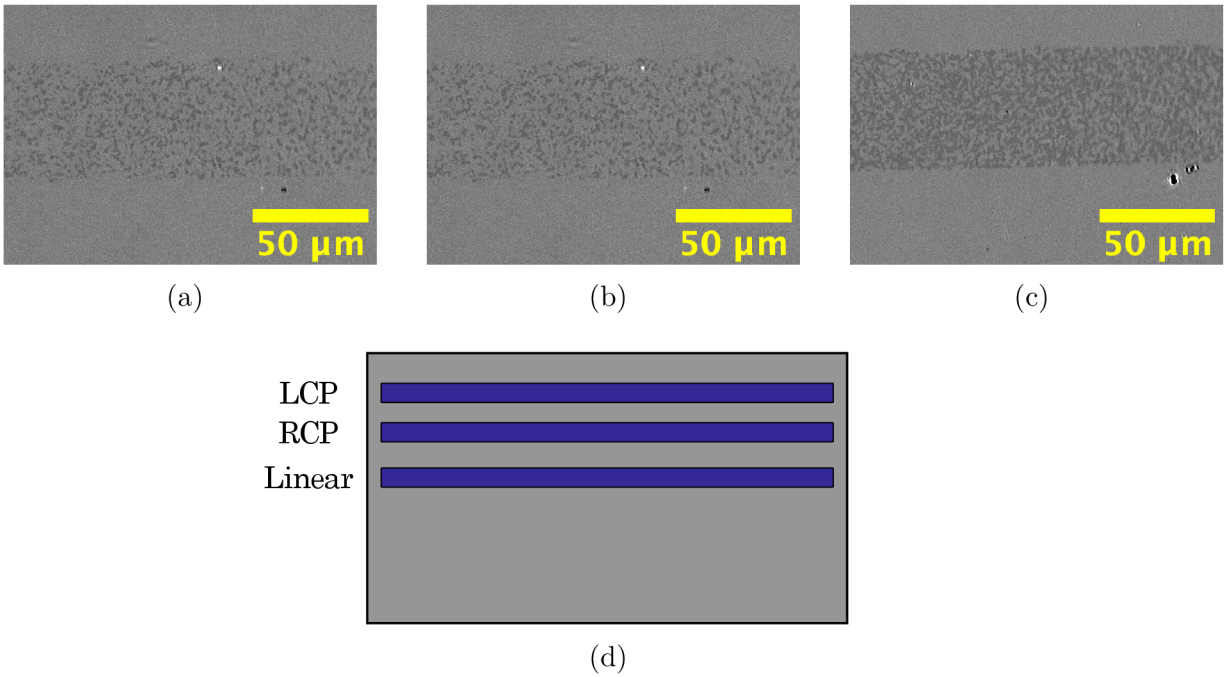

Figure 5.2: Laser scanned across [Co(1)/Gd(3)] sample with 60 nJ per pulse. Three different polarization were used, (a) LCP, (b) linear, (c) RCP. Each with a different absorption, causing domains to occur within area illuminated occur. (d) schematics of the illumination geometry of the sample with different light polarizations.

Conclusion

In this thesis, we explore the basics of magnetism. The energies which are responsible for magnetism and magnetization orientation. This helps us to understand different magnetic orderings further examined. Polarization optics and Jones calculus were discussed in order to understand how light propagates through a medium. Following up on this was the description of magneto-optical effects, specifically the magneto-optical Kerr effect (MOKE). We follow up on MOKE because microscopy based on Kerr effect is an effective tool how to study magnetic materials and their behavior.

We developed a laser setup based on a femtosecond laser source and characterized its main properties. Firstly, we optimize the energy per pulse, then using computer-controlled motors and polarimeter, we identify three polarization states that prove essential for understanding the mechanisms of all-optical switching: left-, right-circular polarization and linear polarization.

Next, we studied the magnetic properties of ferromagnetic [Co/Pt] multilayers and ferrimagnetic stacks of [Co/Gd]. With aforementioned Kerr microscopy we verified the samples crucial properties such as strong perpendicular magnetic anisotropy and square-like hysteresis loop. We observed a domain formation for different thicknesses of Co $t_{\mathrm{Co}} = 0.4\,\mathrm{nm}, 0.6\,\mathrm{nm}$ in $[\mathrm{Co/Pt}]_N$ multilayers and repetition rates of $N = 1$, 3 and 8. The size of domains decrease with increasing number of repetitions.

Three different thicknesses of Co in [Co/Gd] multilayer were examined $t_{Co} = 1\,\mathrm{nm}$, $1.2\,\mathrm{nm}$ and $1.4\,\mathrm{nm}$. Samples with $t_{Co} > 1\,\mathrm{nm}$ showed weak perpendicular magnetic anisotropy, meaning the sample would break in oppositely magnetized domains at zero field. For the thickest sample no formation of domain was visible at zero field.

Using the laser setup, we were able to perform experiments for ultrafast control of magnetization, both on [Co/Pt] multilayer (ferromagnet) and [Co/Gd] multilayer (ferrimagnet). For Co/Pt we showed all-optical helicity-dependent switching (HD-AOS) of magnetization. Meaning that light can selectively change magnetization, depending on its helicity. We show that for ferrimagnetic Co/Gd we observe helicity independent all optical switching (HI-AOS) indicating, that polarization does not play a role in determining the final magnetization orientation of the switched areas. From pictures showing the results, we observe different absorption of light due to magnetic circular dichronism.

Described experiments were done by scanning the laser at low speed across the sample. For future development would be interesting to perform single-pulse experiments. We can further develop the setup by implementing a microscope to perform *in-situ* experiments. Another expansion might include time-resolved experiments, using a pump-probe layout.

References

1. BEAUREPAIRE, E.; MERLE, J.-C.; DAUNOIS, A.; BIGOT, J.-Y. Ultrafast Spin Dynamics in Ferromagnetic Nickel. *Phys. Rev. Lett.* 1996, vol. 76, no. 22, pp. 4250–4253.
2. KIRILYUK, A.; KIMEL, A. V.; RASING, T. Ultrafast optical manipulation of magnetic order. *Rev. Mod. Phys.* 2010, vol. 82, no. 3, pp. 2731–2784.
3. STANCIU, C. D. et al. All-Optical Magnetic Recording with Circularly Polarized Light. *Phys. Rev. Lett.* 2007, vol. 99, no. 4, p. 047601.
4. RADU, I. et al. Transient ferromagnetic-like state mediating ultrafast reversal of antiferromagnetically coupled spins. *Nature*. 2011, vol. 472, no. 7342, pp. 205–208.
5. EL HADRI, M. S E.; HEHN, M.; MALINOWSKI, G.; MANGIN, S. Materials and devices for all-optical helicity-dependent switching. *J. Phys. D: Appl. Phys.* 2017, vol. 50, no. 13, p. 133002.
6. LALIEU, M. L. M.; PEETERS, M. J. G.; HAENEN, S. R. R.; LAVRIJSEN, R.; KOOPMANS, B. Deterministic all-optical switching of synthetic ferrimagnets using single femtosecond laser pulses. *Phys. Rev. B*. 2017, vol. 96, no. 22, p. 220411.
7. LAMBERT, C-H. et al. All-optical control of ferromagnetic thin films and nanostructures. *Science*. 2014, vol. 345, no. 6202, pp. 1337–1340.
8. ALEBRAND, S. et al. Light-induced magnetization reversal of high-anisotropy TbCo alloy films. *Appl. Phys. Lett.* 2012, vol. 101, no. 16, p. 162408.
9. MANGIN, S. et al. Engineered materials for all-optical helicity-dependent magnetic switching. *Nature Mater*. 2014, vol. 13, no. 3, pp. 286–292.
10. SPALDIN, N. A. *Magnetic materials: fundamentals and applications*. Cambridge university press, 2010.
11. COEY, J. M. D. *Magnetism and magnetic materials*. Cambridge; New York: Cambridge University Press, 2009. ISBN 978059780511845000.
12. CULLITY, B.D.; GRAHAM, C.D. *Introduction to Magnetic Materials*. Wiley, 2009. ISBN 978-0-471-47741-9.
13. BINNS, C. Chapter 9 - MAGNETISM AT SURFACES AND INTERFACES. In: NALWA, Hari Singh (ed.). *Handbook of Surfaces and Interfaces of Materials*. Burlington: Academic Press, 2001, pp. 357–392. ISBN 978-0-12-513910-6.
14. FOWLES, G.R. *Introduction to Modern Optics*. Dover Publications, 1989. Dover Books on Physics Series. ISBN 978-0-486-65957-2.
15. SALEH, B.; TEICH, M. *Fundamentals of Photonics, 3rd Edition*. 2019. ISBN 978-1-119-50687-4.
16. SCHÄFER, R. Investigation of Domains and Dynamics of Domain Walls by the Magneto-optical Kerr-effect. In: 2007. ISBN 978-0-470-02218-4.
17. KUCH, W.; SCHÄFER, R.; FISCHER, P.; HILLEBRECHT, F. U. *Magnetic Microscopy of Layered Structures*. Springer, 2014. ISBN 978-3-662-44532-7.
18. SOLDATOV, I. V.; SCHÄFER, R. Selective sensitivity in Kerr microscopy. *Review of Scientific Instruments*. 2017, vol. 88, no. 7, p. 073701.

19. COHERENT, Inc. *Monaco system datasheet* [online] [visited on 2022-05-10]. Available from: https://content.coherent.com/legacy-assets/pdf/COHR_Monaco1035_DS_0120_1.pdf.

20. COHERENT, Inc. *Opera system datasheet* [online] [visited on 2022-05-10]. Available from: https://content.coherent.com/legacy-assets/pdf/COHR_Opera-F_DS_0919_1.pdf.

21. BALTZ, V.; MARTY, A.; RODMACQ, B.; DIENY, B. Magnetic domain replication in interacting bilayers with out-of-plane anisotropy: Application to Co/Pt multilayers. *Phys. Rev. B.* 2007, vol. 75, no. 1, p. 014406.

22. TALAPATRA, A.; MOHANTY, J. Magnetic domain and domain wall in Co/Pt multilayer. *AIP Conference Proceedings*. 2016, vol. 1731, no. 1, p. 130027.

List of abbreviations

AOS	All-optical switching
BS	Beamsplitter
HD	Helicity-dependent
HI	Helicity-independent
LCP	Left-circular polarization
MOKE	Magneto-optical Kerr effect
PMA	Perpendicular magnetic anisotropy
QWP	Quarter-wave plate
RCP	Right-circular polarization
SHG	Second-harmonic generation